Clim. Past Discuss., 7, 2061–2088, 2011
www.clim-past-discuss.net/7/2061/2011/
doi:10.5194/cpd-7-2061-2011

Climate of the Past Discussions

Volcanic and ENSO effects in China in simulations and reconstructions: Tambora eruption 1815

D. Zhang[1,2,3], **R. Blender**[1], **and K. Fraedrich**[1]

[1]Meteorologisches Institut, KlimaCampus, Universität Hamburg, Germany
[2]Institute of Geographic Sciences and Natural Resources Research, Chinese Academy of Sciences, Beijing, China
[3]Graduate School of the Chinese Academy of Sciences, Beijing, China

Received: 9 June 2011 – Accepted: 16 June 2011 – Published: 22 June 2011

Correspondence to: R. Blender (richard.blender@zmaw.de)

Published by Copernicus Publications on behalf of the European Geosciences Union.

Abstract

The co-operative effects of volcanic eruptions and ENSO (El Niño/Southern Oscillation) on the climate in China are analyzed in a millennium simulation for 800–2005 AD using the earth system model (ESM) ECHAM5/MPIOM/JSBACH subject to anthropogenic and natural forcings. The experiment includes two ensembles with weak (5 members) and strong (3 members) total solar irradiance variability. In the absence of El Niño and La Niña events, volcanoes, which are the dominant forcing in both ensembles, cause a dramatic cooling in West China (−2 °C) and a drought in East China during the year after the eruption. The recovery times for the volcano induced cooling vary globally between one and 12 yr; in China these values are mostly within 1–4 yr, but reach 10 yr in the Northeast. Without volcanoes, after El Niño events the summer precipitation is reduced in the North, while South China becomes wetter (indicated by the Standardized Precipitation Index, SPI, for summers, JJA); La Niña events cause opposite effects. El Niño events in the winters after eruptions compensate the cooling in most regions of China, while La Niña events intensify the cooling (up to −2.5 °C). The simulated impact of the eruption of the Tambora in 1815, which caused the "year without summer" 1816 in Europe and North America and coldness and famines for several years in the Chinese province Yunnan, depends crucially on the ENSO state of the coupled model. A comparison with reconstructed El Niño events shows a moderate cool climate with wet (in the South) and extreme dry anomalies (in the North) persisting for several years.

1 Introduction

Volcanic eruptions are the dominant external climate perturbations on the interannual time scale since the stratospheric dust veils reduce temperature for years and alter summer precipitation patterns globally (Angell et al., 1985; Dai et al., 1991; Santer et al., 2001; D'Arrigo et al., 2009; Timmreck et al., 2009). In the temperature record

the most intense eruptions are detectable while impacts on precipitation and pressure are less clear (Mass and Portman, 1989). In general the winter temperature after an eruption is above normal in North America and Eurasia whereas North Africa and Southeast Asia are cooler (Robock and Mao, 1995; Thompson et al., 1995).

While the majority of analyses of the post-volcanic climate pertain to Europe and North America, less is known about China/East Asia although there is a wealth of reconstructions and documentary sources (for a review on volcanic impacts during 1200–1700 AD see Atwell, 2001). In Northeast China a cooling and drying is found after volcanic eruptions (Mao et al., 2009). In Southeast Asia transitions from wetter conditions during the eruption year towards drier conditions after the eruption are found (Anchukaitis et al., 2010). Drought in East China during the eruption and the subsequent year is confirmed in a simulation by Peng et al. (2010).

The recovery of the climate after an abrupt external perturbation like a volcanic eruption proceeds on time scales determined by the memory of land surface and ocean. This time scale determines the accumulative effect of climate anomalies and is, for example, relevant for precipitation deficits. Robock and Mao (1995) find a time scale of two years in 140 yr observations. In a model simulation Robock and Liu (1994) detected a time scale of four years for the relaxation of temperature to climatological means and less than three years for precipitation. After the most intense volcanic eruptions of the last millennium, 1258 (unknown) and in 1815 (Tambora), the cold temperature anomalies recovered on decadal time scales, which is attributed to the ocean heat uptake in a coupled ensemble experiment (Stenchikov et al., 2009). During the Dalton minimum (1790–1830) at the end of the Little Ice Age a series of volcanic eruptions occurred which lowered temperature persistently since the oceanic mixed layer could not recover (Crowley et al., 2008; Cole-Dai et al., 2009). Few results are available about the recovery in complex coupled atmosphere-ocean-general-circulation models (AOGCMs) on a regional scale.

Based on observed correlations between volcanic eruptions and El Niño events, it was suggested that eruptions might trigger El Niño events (for a discussion see

Adams et al., 2003). Such impact is highly relevant for Southeast Asia since the El Niño/Southern Oscillation (ENSO) is related to drought during El Niño and wetness during La Niña phases. Due to these impacts both phenomena can lead to either a partial cancellation or to an enhancement with even more disastrous consequences. In perpetual January GCM experiments Kirchner and Graf (1995) observe that the combined signal of volcanic eruptions and ENSO differs from a linear combination of the separate signals. In proxy data after 1649 Adams et al. (2003) find evidence for a two-fold increase of the probability for an El Niño-like response to a volcanic eruption. Emile-Geaye et al. (2008) consider the triggering hypothesis in paleoclimate data and in simulations with an intermediate complexity model and find that only eruptions with the intensity of at least the Mt. Pinatubo in 1991 can enhance the likelihood for a subsequent El Niño event (by 50 %).

Since reliable reconstructions of past El Niño events are restricted to the last three centuries (Quinn et al., 1993), AOGCM simulations are necessary to retrieve reliable correlations and possible causal relationships. However, using a comparison with reconstructions Anchukaitis et al. (2010) conclude that earth system models (ESM) are not yet able to simulate the impact of intense volcanic eruptions. As a major uncertainty the parameterization of aerosol microphysics has been identified by Timmreck et al. (2010).

The most intense eruption in historic time was Tambora in 1815 (Rampino, 1982; Stothers, 1984) which caused the "year without summer" in North America and Europe with dramatic consequences for food supply and health (Oppenheimer, 2003; Soon and Yaskell, 2003). In agreement with other volcanoes located in the tropics, the Tambora impact was global (D'Arrigo et al., 2009). Documentary reports exist in China which describe disasters in various regions after 1815 (Yang et al., 2005): In the province Yunnan (in the South), there was a three years famine (1815–1817) due to a poor harvest of rice and maize caused by low summer and autumn temperatures (anomalies range $-2 \ldots -3\,^{\circ}\mathrm{C}$). In the province Hainan Dao a dry and cold winter is documented for 1815–1816 and in Taiwan and Zhanghua uncommon ice storms with "thick ice on

the road" have been reported in December. Summer snowfall was observed at various locations in Shuangcheng (in the Northeast, now in the Heilongjiang province) and in the provinces Jiangxi and Anhui (both in the South). Cold anomalies have also been found in the eastern parts of China, including the Yangtze River catchment, but famines are not documented in these regions. In the decade after 1815, frequent and strong fluctuations of wet and arid conditions occurred in China, and increased numbers of floods and droughts are reported in the Yangtze delta (Jiang et al., 2005). Since famines and social disasters might have different causes (warm or cold, wet or dry) an analysis of past temperature and precipitation anomalies on a regional scale yields useful hints to understand the evolution of historical events and to adapt to future natural catastrophes.

The aim of this publication is to assess the impacts and the co-operative effects of volcanic eruptions and ENSO events in an ensemble climate simulation for the last 1200 yr with a complex atmosphere-ocean-land model. Two ensembles with different solar forcing reconstructions with eight members in total are available. The patterns of the temperature response and the relaxation time scale are determined for the 21 most intense eruptions. Precipitation anomalies are analyzed in terms of the summer mean monthly Standardized Precipitation Index (SPI). A further focus of this publication is an analysis of the climate after the Tambora eruption (1815) to detect causes for famines reported in China/Southeast Asia. As the eruptions in the ESM ensemble simulation concurred with different simulated ENSO states, a selection of an optimal combination is possible by comparing the model results with documented El Niño events (compare Goosse et al., 2006).

2 Simulated data and analysis

The present analysis is based on the millennium experiments using the COSMOS-Atmosphere-Land-Ocean-Biogeochemistry (ASOB) Earth System Model ("millennium run", Jungclaus et al., 2010). The model includes the atmospheric model ECHAM5

(Roeckner et al., 2003), the ocean model MPIOM (Marsland et al., 2003) and modules for land vegetation (JSBACH, Raddatz et al., 2007) and ocean biogeochemistry (HAMOCC, Wetzel et al., 2006), which are coupled via the OASIS3 coupler. Anthropogenic land-use is prescribed (Foley et al., 2003; Pongratz et al., 2008). ECHAM5 is run at T31 resolution (≈3.75° × 3.75°) with 19 vertical levels, and MPIOM at a horizontal grid spacing of about 3° with 40 unevenly spaced vertical levels.

Two reconstructed Total Solar Irradiance (TSI) forcings are used to produce two ensembles: ensemble E1 (five members) is simulated with the solar irradiance forcing reconstructed by Krivova et al. (2007) with a weak (0.1 %) variation (see Fig. 1a) and a second ensemble E2 (three members) with a more intense (0.25 %) variation, comparable to previous reconstructions (for example Bard et al., 2000), which assume higher magnitudes of TSI variations. Zhang et al. (2010) compared both ensembles with climate reconstructions in China and concluded that ensemble E1 (weak TSI variability) reproduces the reconstructed climate variability; therefore, the present analysis is restricted to this five member ensemble E1 unless indicated otherwise. A control simulation with the same model setup revealed that ENSO is highly correlated with the South and East Asian monsoons (Blender et al., 2010).

The volcanic forcing is represented in terms of the aerosol optical depth and the effective radius distribution (Crowley, 2008). In the simulation (Jungclaus et al., 2010) this forcing is resolved in four latitude bands (30–90° N, 0–30° N, 0–30° S, 30–90° S) with a temporal resolution of 10 days (Fig. 1b, c). In the annual forcing series, 21 large volcanic eruptions are defined (see Table 1) with the strongest reduction in solar irradiance (for detailed reviews on past eruptions see Newhall and Self (1982); Peng et al. (2010); Global Volcanism Program, Smithsonian National Museum of Natural History/Washington). The lowest reduction in this set is $-2.0\,\mathrm{W\,m^{-2}}$ from Santa Maria in Guatemala in 1903 (average of all eight simulations), which is slightly larger than $-1.7\,\mathrm{W\,m^{-2}}$ according to observations. The 1258 giant volcanic eruption (unknown volcano) causes a maximum reduction of radiation between −16.4 and $-16.9\,\mathrm{W\,m^{-2}}$ in all eight simulations. As in Peng et al. (2010) the year with the largest reduction

in irradiance is defined as the volcanic eruption year. This definition can lead to a discrepancy between observation years and eruption years in the present analysis, since the aerosol layer accumulates leading to a delayed response (in some cases associated with a shift of the eruption year). The analysis is performed during the years after the eruptions. Intensity and latitude of the volcanoes are not considered.

ENSO is characterized by the Southern Oscillation Index (SOI), given by the principal component time series (PC1) of the first EOF of the tropical Pacific sea surface temperature (SST) variability in winter (DJF) (see Hoerling et al., 2001). El Niño events are given for SOI > 1, La Niña events for SOI < -1, and a neutral state for $|\mathrm{SOI}| < 1$. The SOI is highly correlated with the NINO3 index ($r = 0.98$). To determine the cooperative effects of volcanic eruptions and ENSO anomalies, composite analyses are performed for the years after eruptions. ENSO events are considered during the winter (DJF) at the end of the eruption year. In the present publication precipitation anomalies are analyzed in terms of the monthly Standardized Precipitation Index (SPI) averaged for summer (JJA), see Sienz et al. (2007).

3 Eruption and ENSO induced climate anomalies

The impacts of eruptions and ENSO events can influence the climate on similar time scales and with comparable magnitudes. Therefore, in order to assess both impacts they are considered separately avoiding years with overlaps: first the climate during the year after an eruption for neutral winter SOI (no ENSO event) is considered; here the averaged time scale and the amplitude of the temperature anomaly is determined globally. Secondly, the simulated ENSO impact in East Asia is determined during years without preceding eruptions. The final analysis considers years in the ensemble simulations with concurrent eruptions and ENSO events.

3.1 Volcanic response without ENSO events

The response of temperature and precipitation anomalies during the year after a volcanic eruption is first considered without ENSO events during two preceding winters, this leads to 31 eruption years in total in ensemble E1 (22 yr in Ensemble E2).

3.1.1 Temperature and precipitation anomalies

Volcanoes cool East Asian, especially the high altitude Himalayan region in West China with anomalies as low as $-1\,^{\circ}\mathrm{C}$ in average (Fig. 2a for ensemble E1). The mean in China is $-0.54\,^{\circ}\mathrm{C}$ ($-0.53\,^{\circ}\mathrm{C}$ in ensemble E2). During the year of the eruption the temperature anomaly reaches $-0.54\,^{\circ}\mathrm{C}$ in E1 (E2: $-0.38\,^{\circ}\mathrm{C}$). The anomalies in both years are significant.

Central China experiences anomalous wet summer (JJA) conditions (determined by the summer mean SPI) while a weak drought prevails in the South and the Northeast of China (Fig. 3a). The average summer rainfall anomaly in China during the year after the eruption is -56 mm in E1 (-43 mm in E2). In the eruption year (not shown) the anomaly is -47 mm in E1 (-43 mm in E2). Mao et al. (2009) report cool and dry periods after 11 volcanic eruptions. The rainfall deficit after the eruption year is 85 %-significant in our analysis (a rainfall anomaly is also found by Fisher et al. (2007), Anchukaitis et al. (2010), and Peng et al. (2010)).

3.1.2 Recovery timescale

The recovery of the local temperature drop after an eruption is described in terms of an exponential function, $\Delta T(t) = \Delta T_0 \exp(-t/\tau)$, beginning with the first year after the eruption ($t = 0$) and ending at $t = 10$ yr (see Fig. 4 for two examples of fitted temperature episodes). At every grid box, the amplitude ΔT_0 and the time scale τ are fit parameters for the average of the temperature relaxation anomalies.

The global distribution of the fitted decay amplitudes ΔT_0 and the relaxation time scales τ are included in Fig. 5a and b at grid points where fits can be achieved (Ensemble E2 reveals similar results, not shown). Note that this amplitude is the result of a fit and not identical to the anomaly during the year after the eruption (see Fig. 2a). Land and ocean reveal similar amplitudes. Large amplitudes reaching −2 °C are found in North America, the Himalaya, and the Barents Sea, and in the Southern Pacific Ocean between 160° W–60° W. Areas with negligible amplitudes inhibit fits (void in Fig. 5a, b); furthermore areas with weak positive amplitudes (mostly in the tropical Pacific, the Bering Sea, and in parts of the Southern Pacific) are excluded.

The recovery time scales τ (Fig. 5b) reveal a long-lasting influence up to a decade in Southern Europe, Northeast China and in the Arctic Ocean. In China the time scales are mostly within 1–4 yr and reach 10 yr in the Northeast. A remarkable coincidence of high amplitudes and large time scales appears in the Southern Pacific Ocean between 160° W–60° W.

A possible physical mechanism for small amplitudes and short time scales on the ocean is rapid mixing in the ocean surface layer. In regions with small amplitudes intense long term memory has been identified in preceding analyses of the global sea surface temperature (Fraedrich and Blender, 2003).

3.2 ENSO impact without preceding eruptions

The impacts of winter El Niño and La Niña events on temperature and precipitation anomalies in the subsequent year are almost anti-symmetric (determined in ensemble E1, Fig. 2b, c, Fig. 3b, c); in this analysis, years with a preceding volcanic eruption are excluded. El Niño warms the largest part of East Asia except for the Northeast and temperature anomalies up to +1 °C are simulated in India and Southeast Asia (opposite for La Niña, Fig. 2c). The summer mean SPI for El Niño events shows a tripole pattern oriented from Southwest to the Northeast (Fig. 3b, c): Whereas Southeast Asia experiences moderate summer wetness, India and Northeast China are drier (the La

Niña impact is almost opposite). Clearly, the dominant impact is in the western tropical Pacific.

3.3 Volcanic response with ENSO events

Among the 105 volcanic eruptions in Ensemble E1 (E2: 63), 46 (24) are accompanied by ENSO events in the following winter (equal numbers of El Niños and La Niñas). The sum of El Niño events amounts to 1249 (733) and La Niñas events to 1164 (704). A significant increase of El Niño events after volcanic eruptions is not found in both ensembles; the p-values are 0.81 for El Niños in E1 (E2: 0.84), and 0.59 for La Niñas in E1 (E2: 0.94).

The temperature and SPI responses during the year after volcanic eruptions with a winter El Niño or La Niña event may reveal dramatic impacts. In China the cooling effect caused by volcanic eruptions (Fig. 2a) is almost compensated by the warming induced by El Niño events (Fig. 2d). The superposition of the La Niña and the volcano impact (Fig. 2e) yields enhanced cooling by the same order of magnitude. In the Northern Pacific the La Niña induced warming dominates. After the eruption with an accompanying El Niño event the temperature anomaly in experiment E1 is −0.12 °C (experiment E2: −0.31 °C) and for a La Niña event −0.73 °C in E1 (E2: −0.68 °C).

The co-operative precipitation response of volcanoes and El Niños (Fig. 3d) reveals a quasi-linear superposition with a dominance of the El Niño pattern shaped as a tripole (Fig. 3b). In west and central China wetness caused by volcanic eruptions is unaltered by El Niños; in the North dryness is even stronger in the combined case (Fig. 3d) than in the pure volcano or El Niño response. A similar superposition pertains to La Niña (Fig. 3e). Remarkable is that in West China (province Xinjiang), the volcano induced wetness is absent after La Niña events, although La Niña events do not cause dryness here. Thus, the major mutual interaction of volcanoes and ENSO anomalies can be understood as a linear superposition, with a few deviations, mainly in West China, which can possibly be interpreted as nonlinearities. The SPI (JJA) anomalies obtained in the second ensemble E2 (not shown) show similar results. The average summer

rainfall anomaly in China in years after an eruptions and a subsequent El Niño event in Ensemble E1 is −64 mm (E2: −68 mm); for a subsequent La Niña event the anomaly is even positive with +29 (+29) mm.

4 Tambora eruption in 1815

The eruption of the Tambora during April 1815 was the most intense eruption in historic times classified by the Volcanic Explosivity Index VEI=7 (on a scale from 0 to 8, see also Table 1). The Tambora eruption occurred during the Dalton minimum (1790–1830), an extreme cold period terminating the Little Ice Age and caused the "year without summer" 1816. In the present simulations the Tambora eruption is the second most intense with a drop in solar radiation of −6.9 to −7.5 $W m^{-2}$ detected in the eight ensemble members.

The Tambora eruption caused a long cold period in China. The temperature reduction (Fig. 6a) during the period 1780–1850 is clearly visible in the simulated annual mean temperature anomaly and in the reconstructions by Wang et al. (2007) and Yang et al. (2002). The cooling started in 1809 (eruption of St. Helen) and reached an anomaly between −1.2 and −1.3 °C in the two ensembles. The simulated anomalies reveal a recovery time scale of several years, which is distinctly longer than the mean calculated for 31 eruptions (Fig. 5b). Note that the temperature drop after the Tambora eruption is larger than the mean in most parts of China (Fig. 5a).

The simulated summer (JJA) SPI in Southeast China (105° E–130° E, 25–30° N, as in the reconstruction by Zheng et al., 2006) is below the mean for more than two decades, 1795–1825, in both simulations, which add up to a climatological relevant humidity deficit at the end of the Dalton minimum (Fig. 6b). The reconstruction of an annual dry/wet index by Garnaut (2010) reveals high intra-annual variability and no relationship to the eruption in 1815. The decadal reconstructed dry/wet summer index by Zheng et al. (2006) based on historical documents reveals a depression during the Dalton Minimum which is neither reflected in the Garnaut index nor in the simulation.

A closer look at the SPI time series in the eight experiments reveals that there is a possible likelihood for decreased precipitation after 1815. Its variability can be explained by ENSO (see Fig. 3b, c). Therefore, the eight SOI time series in the period near the eruption (Fig. 7a) are compared to historic documents. Furthermore, extreme La Niña and El Niño as well as a neutral case are considered.

According to the reconstructed El Niño data (Quinn et al., 1993) there were no El Niño events in 1815 and 1816, but probably strong El Niño events in 1814 and 1817. For a comparison, four simulations with different SOI states are selected out of the eight members in the ensembles E1 and E2: (i) a neutral SOI in 1813-1816 (simulation E1-3), (ii) a strong El Niño in 1816 (E1-4), (iii) a strong La Niña in 1816 (E1-2), and (iv) an optimal realization which follows the historically reconstructed El Niño events closely during 1814–1817 (E2-3, Fig. 7a). Note that due to the absence of information about La Niña events, the reconstruction by Quinn et al. (1993) does not exclude La Niña events to have occurred in 1815 and 1816.

These selected simulations reveal distinct patterns of temperature and precipitation anomalies in China during the decade 1810–1820 (Fig. 7b, c). A remarkable result is that the coldest simulated temperature anomalies for the optimal realization of the SOI did not occur in 1816, but two years after the eruption, with a magnitude similar to the La Niña state. This persistence may explain long lasting impacts like the three years famine in the province Yunnan.

Spatial anomalies of temperature and precipitation corresponding to the four SOI states reveal different response patterns in East Asia in 1816 (Fig. 8). (i) The neutral SOI pattern shows a moderate cooling (compare with Fig. 2a) except in Tibet, Northeast, and Southeast China. The major impact is an extreme dryness in East China (compare Fig. 3a); there is agreement with reconstructions in Northeast China (Mao et al., 2009). (ii) The El Niño pattern (which is unlikely according to the reconstruction by; Quinn et al., 1993) balances the volcanic cooling and the dryness effects in large parts of China (Fig. 4d). (iii) A La Niña state generates extreme coldness in East Asia and a moderate drought in the South and the Northeast (the strong volcano dominates

the La Niña impact, compare Fig. 3a, c); note that these regions are the most densely inhabited areas in China. (iv) The realization with the optimal SOI pattern reveals a moderate cold anomaly in a large part of China (besides the South) and an extreme dryness in the Northeast.

Comparison of the simulation with historical documents excludes an El Niño event in the winter 1815/1816 for two reasons (in agreement with Quinn et al., 1993): First, observations report coldness in most parts of China while the El Niño simulation does not indicate a temperature anomaly. Secondly, the documents describe droughts in the East as it is simulated by all SOI states besides El Niño. However, a caveat remains for the simulation with the optimal SOI (which is close to reconstructions) since the simulated wetness and the absence of a temperature anomaly in Southeast China contradict historical documents reporting a dry and cold period. A general conclusion is that temperature is dominated by the El Niño event, while precipitation remains dominated by the impact of the Tambora eruption.

5 Summary and discussion

Due to the high population density China is extremely vulnerable to the climate impacts of volcanic eruptions, in particular if at the same time East Asia is influenced by El Niño/Southern Oscillation (ENSO) events which may amplify (but also mitigate) the anomalies caused by eruptions. The present analysis uses ensemble simulations with a comprehensive state of the art Earth System Model (ESM) to (i) determine the impact of eruptions on temperature and summer precipitation anomalies (characterized by the Standardized Precipitation Index, SPI), (ii) estimate the recovery time scale of temperature anomalies, and (iii) analyze the correlations and the co-operative effects of volcanoes and ENSO. Focus of this study is the Tambora eruption (1815) which had similar social impacts in China as the "year without summer" in Europe and North America. The ENSO state in different ensemble members is compared to historic information in 1814–1817 to select an optimal realization of the simulated climate.

The climate is simulated for 800–2005 AD by the COSMOS ASOB earth system model in a millennium run including ECHAM5 in T31/L19, MPIOM in GR3.0/L40 resolution and the JSBACH land module subject to anthropogenic and natural forcings. Two ensembles are produced by applying two different reconstructions of Total Solar Irradiance (five members for weak and three members for strong variability). The simulations use forcings for volcanic aerosols and anthropogenic forcings (land-cover-changes and greenhouse gas emissions).

For the present analysis the most intense 21 volcanic eruptions are selected to determine volcanic and ENSO impacts on the climate in China. ENSO is characterized by the Southern Oscillation Index (SOI), defined by the principal component time series (PC1) of the first EOF of the tropical Pacific sea surface temperature (SST) variability in winter (DJF). The results show that volcanoes cause a dramatic cooling in West China accompanied by drought in the eastern parts of China during the year after eruption. The mean temperature is reduced by $-0.54\,^{\circ}\mathrm{C}$ in China and summer precipitation decreases by about -45 mm.

The recovery times of the cooling which describe the accumulated impact of the eruptions is determined locally by an exponential function, $\Delta T_0 \exp(-t/\tau)$, with an amplitude ΔT_0 and a time scale τ. The recovery time varies between one and 12 yr globally with the shortest times found on the oceans. In China the cooling decays mostly within 1-4 yr, in the Northeast, however, 10 yr are detected. Note that in some ocean basins the cooling ΔT_0 is too weak to fit an exponential decay.

An El Niño event (defined by $\mathrm{SOI} < -1$) warms most regions in China by about $+0.5\,^{\circ}\mathrm{C}$; cooler temperatures are found in the Northeast. The summer precipitation decreases in the North, while South China becomes wetter after El Niño events. La Niña events cause opposite effects for temperature and precipitation. In the present simulation, the occurrence of El Niño events is not significantly increased after volcanic eruptions. Note, however, that this result is in disagreement with reconstructions (Adams et al., 2003) and might be a model specific property.

The combined signal of volcanoes and ENSO cannot be considered as a linear superposition of two distinct signals. EL Nino events after eruptions yield moderate temperature anomalies in China, in particular the volcano induced cooling in the West is almost compensated by El Niño and the precipitation deficit in the Southeast is inhibited. La Niña events, however, intensify the cooling (anomalies up to −3 °C) and the drought in Southeast Asia.

The Tambora eruption in 1815 occurred during the Dalton Minimum (1790–1830), an extremely cold period at the end of the Little Ice Age. Simulated temperature and SPI are compared with the reconstructed mean temperature in China (Yang et al., 2002; Ge et al., 2003; Wang et al., 2007) and the wet-dry index in Southeast China (Zheng et al., 2006; Garnaut, 2010). The climate response to Tambora depends crucially on the ENSO state of the individual ensemble members. Indeed, one of the simulations yields an ENSO pattern which can be associated with the historical El Niño reconstruction (Quinn et al., 1993; note that La Niña events are not included). This simulation caused a moderate temperature anomaly of −1.2 °C, moderate wetness in south China and extreme drought in the North and the Northeast.

Acknowledgements. We like to thank Johann Jungclaus, Martin Claußen, Xiuhua Zhu, and the Millennium consortium at the Max-Planck Institute and at the University of Hamburg for providing the simulated data and stimulating discussions. We are grateful to Wang Shao-Wu (Beijing) and Ge Quan-Sheng (Beijing) for providing the reconstructed temperature, Zheng Jing-Yun and Anthony Garnaut for the dry/wetness index. DZ acknowledges the support for the visit to KlimaCampus by the Institute of Geographic Sciences and Natural Resources Research (Chinese Academy of Sciences) and KF acknowledges support by Max Planck Society.

References

Adams, J. B., Mann, M. E., and Ammann, C. M.: Proxy evidence for an El Niño-like response to volcanic forcing, Nature, 426, 274–278, 2003.

Anchukaitis, K. J., Buckley, B. M., Cook, E. R., Cook, B. I., D'Arrigo, R. D., and Ammann, C. M.: Influence of volcanic eruptions on the climate of the Asian monsoon region, Geophys. Res. Lett., 37, L22703, doi:10.1029/2010GL044843, 2010.

Angell, J, K. and Korshover, J.: Surface temperature changes following the six major volcanic episodes between 1789 and 1980, J. Clim. Appl. Meteorol., 24, 937–951, 1985.

Atwell, W. S.: Volcanism and short-term climatic change in East Asian and world history, c. 1200–1699, J. World Hist., 12, 29–98, 2001.

Blender, R., Zhu, X. H., Zhang, D., and Fraedrich, K.: Yangtze runoff, precipitation, and the East Asian monsoon in a 2800 years climate control simulation, Quatern. Int., online, doi:10.1016/j.quaint.2010.10.017, 2010.

Cole-Dai, J., Ferris, D., Lanciki, A., Savarino, J., Baroni, M., and Thiemens, M. H.: Cold decade (AD 1810–1819) caused by Tambora (1815) and another (1809) stratospheric volcanic eruption, Geophys. Res. Lett., 36, L22703, doi:10.1029/2009GL040882, 2009.

Crowley, T. J., Zielinski, G., Vinther, B., Udisti, R., Kreutz, K., Cole-Dai, J., Castellano, E.: Volcanism and the Little Ice Age, PAGES News, 16, 22–23, 2008.

D'Arrigo, R., Wilson, R., and Tudhope, A.: The impact of volcanic forcing on tropical temperatures during the past four centuries, Nat. Geosci., 2, 51–56, 2009.

Dai, J., Mosley-Thompson, E., and Thompson, L. G.: Ice core evidence for an explosive tropical volcanic eruption 6 years preceding Tambora, J. Geophys. Res., 96(D9), 17361–17366, 1991.

Emile-Geay, J., Seager, R., Cane, M. A., and Cook, E. R., Haug, G. H.: Volcanoes and ENSO over the past millennium, J. Climate, 21, 3134–3148, 2008.

Foley J. A., Costa, M. H., Delire, C., Ramankutty, N., and Snyder, P.: Green surprise? How terrestrial ecosystems could affect Earth's climate, Front. Ecol. Environ., 1, 38–44, 2003.

Garnaut, A.: Dry/wet index in China for 1470–1979, private communication, 2010.

Ge, Q. S., Zheng, J. Y., Fang, X. Q., Man, Z. M., Zhang, X. Q., Zhang, P. Y., Wang, W. C.: Winter half-year temperature reconstruction for the middle and lower reaches of the Yellow River and Yangtze River, China, during the past 2000 years, Holocene, 13, 933–940, 2003.

Goosse, H., Renssen, H., Timmermann, A., Bradley, R. S., Mann, M. E.: Using paleoclimate proxy-data to select optimal realizations in an ensemble of simulations of the climate of the past millennium, Clim. Dynam., 27, 165–184, doi:10.1007/s00382-006-0128-6, 2006.

Jiang, T., Zhang, Q., Blender, R., and Fraedrich, K.: Yangtze Delta floods and droughts of the last millennium: Abrupt changes and long term memory, Theor. Appl. Climatol., 82, 131–141, 2005.

Jungclaus, J. H., Lorenz, S. J., Timmreck, C., Reick, C. H., Brovkin, V., Giorgetta, M. A., Raddatz, T. J., Roeckner, E., Segschneider, J., Six, K., Schnur, R., Widmann, H., Crowley, T. J., Krivova, N., Vieira, L. E., Solanki, S. K., Klocke, D., Botzet, M., Esch, M., Gayler, V., Haak, H., Pongratz, J., Claussen, M., Stevens, B., and Marotzke, J.: Climate and carbon-cycle variability over the last millennium, Clim. Past, 6, 1009–1044, 2010, http://www.clim-past.net/6/1009/2010/.

Kirchner, I. and Graf, H. F.: Volcanos and El Niño: signal separation in Northern Hemisphere winter, Clim. Dynam., 11, 341–358, 1995.

Krivova, N. A., Balmaceda, L., and Solanki, S. K.: Reconstruction of solar total irradiance since 1700 from the surface magnetic flux, Astron. and Astrophys., 467, 335–346, 2007.

Mao, X., Cheng, S., Hong, Y., Zhu, Y., and Wang, F.: The influence of volcanism on paleoclimate in the northeast of China: Insights from Jinchuan peat, Jilin Province, China, Chin. J. Geochem., 28, 212–219, doi:10.1007/s11631-009-0212-9, 2009.

Marsland, S., Haak, H., Jungclaus, J. H., Latif, M., and Röske, F.: The Max-Planck-Institute global ocean/sea ice model with orthogonal curvilinear coordinates, Ocean Model., 5, 91–127, 2003.

Mass, C. F. and Portman, D. A.: Major volcanic eruptions and climate: a critical evaluation, J. Climate, 2, 566–593, 1989.

Newhall, C. G. and Self, S.: The volcanic explosivity index (VEI): An estimate of explosive magnitude for historical volcanism, J. of Geophys. Res., 87, 1231–1238, 1982.

Oppenheimer, C.: Climatic, environmental and human consequences of the largest known historic eruption: Tambora volcano (Indonesia) 1815, Prog. Phys. Geog., 27, 230–259, 2003.

Peng, Y., Shen, C., Wang, W., and Xu, Y.: Response of Summer precipitation over Eastern China to large volcanic eruptions, J. Climate, 23, 818–824, doi:10.1175/2009JCLI2950.1, 2010.

Pongratz, J., Reick, C., Raddatz, T., and Claussen, M.: A reconstruction of global agricultural areas and land cover for the last millennium, Global Biogeochem. Cy., 22, GB3018, doi:10.1029/2007GB003153, 2008.

Quinn, W. H.: The large-scale ENSO event the El Niño and other important regional features, Bull. Inst. fr. études andines, 22, 13–34, 1993.

Raddatz, T. J., Reick, C. J., Knorr, W., Kattge, J., Roeckner, E., Schnur, R., Schnitzler, K. G., Wetzel, P., and Jungclaus, J. H.: Will the tropical land biosphere dominate the climate-carbon cycle feedback during the 21st century, Clim. Dynam., 29, 565–574, 2007.

Rampino, M. R. and Self, S.: Historic eruptions of Tambora (1815), Krakatau (1883), and Agung (1963), their stratospheric aerosols, and climatic impact, Quatern. Res., 18, 127–143, 1982.

Robock, A. and Liu, Y.: The volcanic signal in Goddard Institute for space studies three-dimensional model simulations, J. Climate, 7, 44–55, 1994.

Robock, A. and Mao, J.: The volcanic signal in surface temperature observations, J. Climate, 8, 1086–1103, 1995.

Roeckner, E., Bäuml, G., Bonaventura, L., Brokopf, R., Esch, M., Giorgetta, M., Hagemann, S., Kirchner, I., Kornblueh, L., Manzini, E., Rhodin, A., Schlese, U., Schulzweida, U., Tompkins, A.: The atmospheric general circulation model ECHAM5. Part I: model description, Max Planck Institute for Meteorology, Report 349, 1–127, 2003.

Santer, B. D., Wigley, T. M. L., Doutriaux, C., Boyle, J. S., Hansen, J. E., Jones, P. D., Meehl, G. A., Roeckner, E., Sengupta, S., and Taylor, K. E.: Accounting for the effects of volcanoes and ENSO in comparisons of modeled and observed temperature trends, J. Geophys. Res., 106(D22), 28033–28059, 2001.

Sienz, F., Bordi, I., Fraedrich, K., and Schneidereit, A.: Extreme dry and wet events in Iceland: observations, simulations and scenarios, Meteorol. Zeitschr., 16, 9–16, 2007.

Soon, W. and Yaskell, S. H.: Year without a summer, Mercury, 32, 13–22, 2003.

Stenchikov, G., Delworth, T. L., Ramaswamy, V., Stouffer, R. J., Wittenberg, A., and Fanrong, F.: Volcanic signals in oceans, J. Geophys. Res., 114, D16104, doi:10.1029/2008JD011673, 2009.

Stothers, R. B.: The great Tambora eruption in 1815 and its aftermath, Science, 224, 1191–1198, 1984.

Thompson, R. D.: Volcanic eruptions and global temperatures, Ambio, 24, 320–321, 1995.

Timmreck, C., Lorenz, S. J., Crowley, T. J., Kinne, S., Raddatz, T. J., Thomas, M. A., and Jungclaus, J. H.: Limited temperature response to the very large AD 1258 volcanic eruption, Geophys. Res. Lett., 36, L21708, doi:10.1029/2009GL040083, 2009.

Timmreck, C., Graf, H. F., Lorenz, S. J., Niemeier, U., Zanchettin, D., Matei, D., Jungclaus, J. H., and Crowley, T. J.: Aerosol size confines climate response to volcanic supereruptions, Geophys. Res. Lett., 37, L24705, doi:10.1029/2010GL045464, 2010.

Wang, S. W., Wen, X. Y., Luo, Y., Dong, W. J., Zhao, Z. C., and Yang, B.: Reconstruction of temperature series of China for the last 1000 years, Chin. Sci. Bull., 52, 3272–3280, 2007.

Wetzel, P., Maier-Reimer, E., Botzet, M., Jungclaus, J. H., Keenlyside, N., and Latif, M.: Effects of ocean biology on the penetrative radiation in a coupled climate model, J. Climate, 19,

3973–3987, 2006.
Yang, B., Bräuning, A., Johnson, K. R., and Shi, Y. F.: General characteristics of temperature variation in China during the last two millennia, Geophys. Res. Lett., 29, 1324–1327, doi:10.1029/2001GL014485, 2002.
Yang, Y. D., Man, Z. M., Zheng, J. Y.: A serious famine in Yunnan (1815–1817) and the eruption of Tambola Volcano (in Chinese), Fudan Journal (Social Sciences), 1, 79–85, 2005.
Zhang, D., Blender, R., Zhu, X. H., and Fraedrich, K.: Temperature variability in China in an ensemble simulation for the last 1200 years, Theor. Appl. Climatol., 103, 387–399, doi:10.1007/s00704-010-0305-8, 2010.
Zheng, J. Y., Wang, W. C., Ge, Q. S., Man, Z. M., and Zhang, P. Y.: Precipitation variability and extreme events in Eastern China during the past 1500 years, Terr. Atmos. Ocean. Sci., 17, 579–592, 2006.

Table 1. List of the selected 21 volcanic eruptions in 800–2005 (eruption year is defined by a decrease in net top solar irradiation of at least $-2.0\,W\,m^{-2}$). The Volcanic Explosivity Index (VEI) is included and question marks indicate uncertainty (Newhall and Steve, 1982; Peng et al., 2010; Global Volcanism Program, Smithsonian National Museum of Natural History/Washington).

No.	Year	Name	VEI
1	842	Unknown	
2	854	Unknown	
3	897	Unknown	
4	971	Unknown	
5	1193	Unknown	
6	1228	Unknown	
7	1258	Unknown	
8	1286	Unknown	
9	1442	Unknown	
10	1456	Pinatubo?	6
11	1600	Huaynaputina	6
12	1641	Parker	6
13	1673	Gamkonora	
14	1694	Serua?/Helka?	
15	1809	St. Helen?	
16	1815	Tambora	7
17	1832	Babuyan Claro	4?
18	1835	Cosiguina	
19	1884	Krakatau	6
20	1903	Santa Maria/2 others	4
21	1992	Pinatubo	6

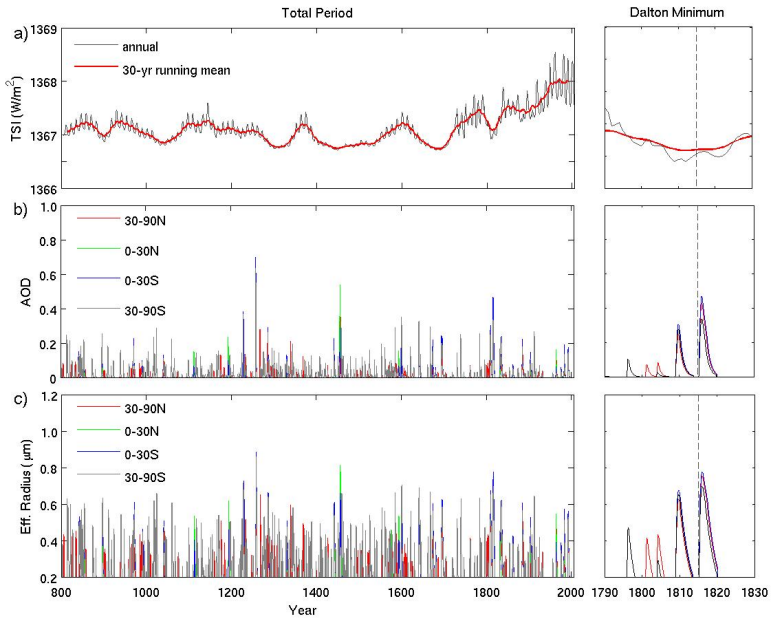

Fig. 1. **(a)** Total solar irradiation in Ensemble E1 (including 30 yr running mean: red) for the whole simulation period (left) and the Dalton minimum (1790–1830, right panel) based on the reconstruction by Krivova et al. (2007), **(b)** Aerosol optical depth (dimensionless fraction), and **(c)** Effective radius [μm], in **(b)** and **(c)** latitude belts are separated. The Dalton Minimum includes the Tambora eruption in 1815 (dashed).

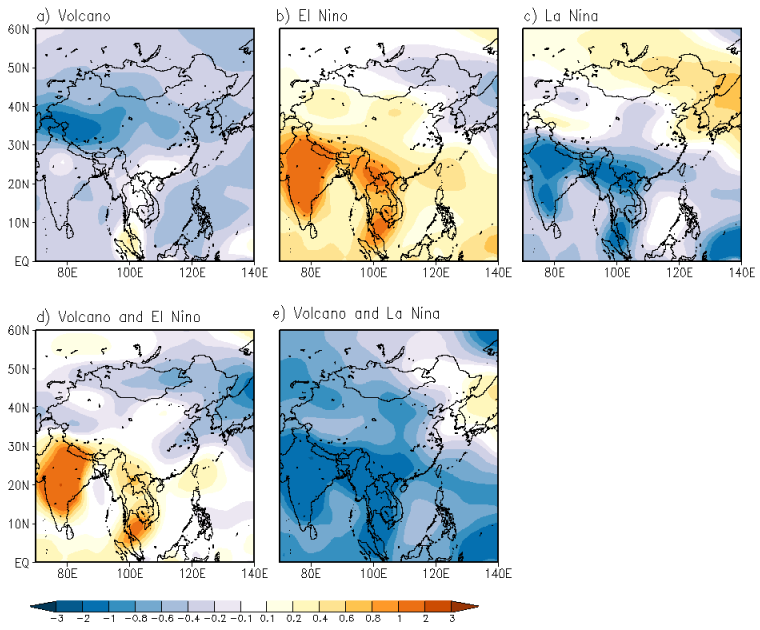

Fig. 2. Temperature anomalies [°C] in the ensemble E1 in the year after volcanic eruptions including ENSO anomalies: **(a)** eruptions with no winter ENSO anomalies (neutral, |SOI| <1), **(b)** El Niño and **(c)** La Niña events without preceding eruption, **(d)** eruptions with El Niño events, **(e)** eruptions with La Niña events.

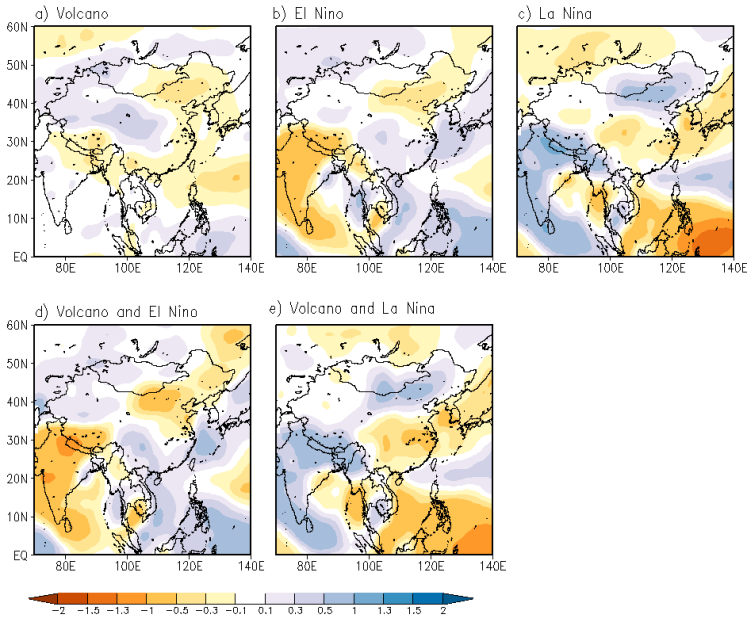

Fig. 3. Summer (JJA) mean of the monthly Standardized Precipitation Index (SPI), see Fig. 2.

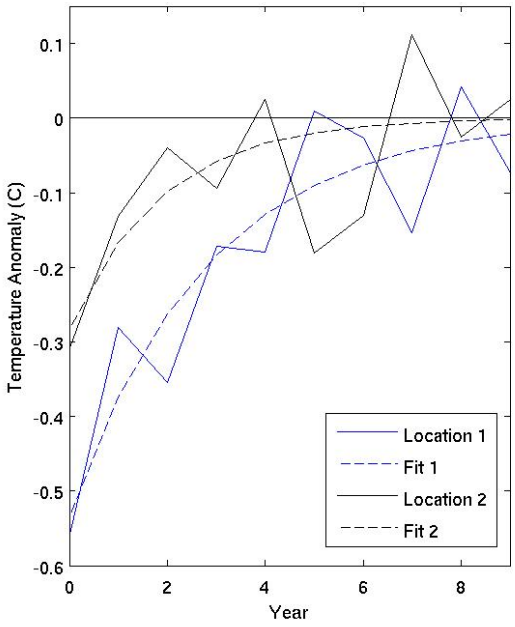

Fig. 4. Examples for two exponential fits to averaged temperature anomalies. Location 1: 102° E/22° N (Northeast China, recovery time scale $\tau \approx 3$ yrs, $\Delta T_0 \approx -0.5$ °C), location 2: 116° E/43° N (Southwest China, $\tau \approx 2$ yrs, $\Delta T_0 \approx -0.3$ °C).

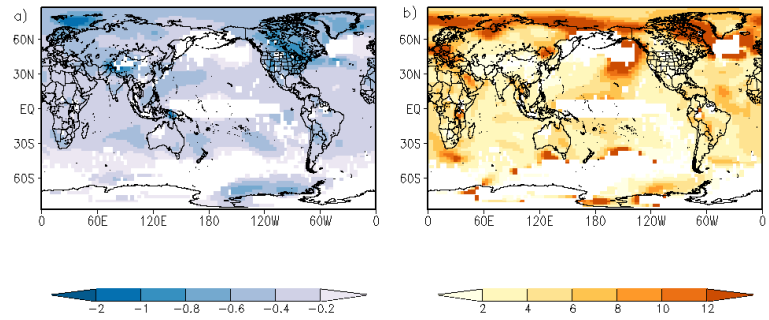

Fig. 5. (a) Temperature decay ΔT_0 and **(b)** relaxation time scale τ for the temperature decay obtained by fits in ensemble E1 for 31 eruptions without El Niño and La Niña events during the preceding two winters.

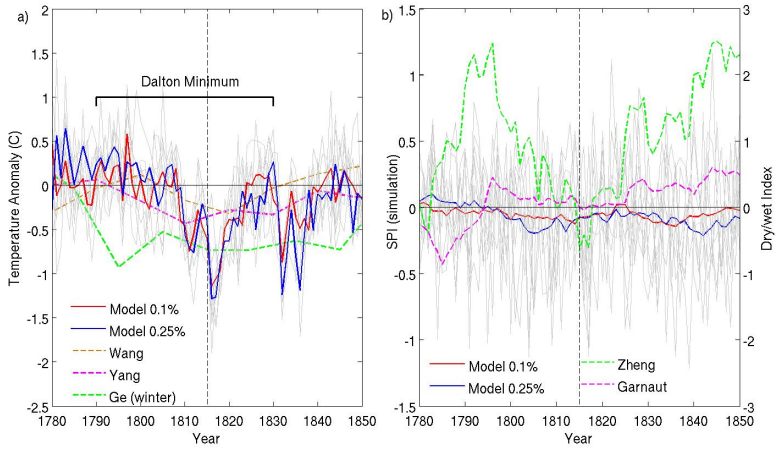

Fig. 6. (a) Temperature anomalies in China in simulations and reconstructions for 1780–1850. The Dalton minimum (1790–1830) and the Tambora eruption (1815) are marked. The simulated (solid) curves are ensemble means for different TSI reconstructions as indicated: thin grey lines indicate all eight ensembles members, and the dashed lines refer to reconstructions by Yang et al. (2002), Ge et al. (2003), and Wang et al. (2007). **(b)** Decadal mean Standardized Precipitation Index (SPI) for summers (solid, as in **(a)**, left axis) and reconstructed dry/wet indices in Southeast China (Zheng et al. (2006) and Garnaut (2010), dashed, decadal means, right axis).

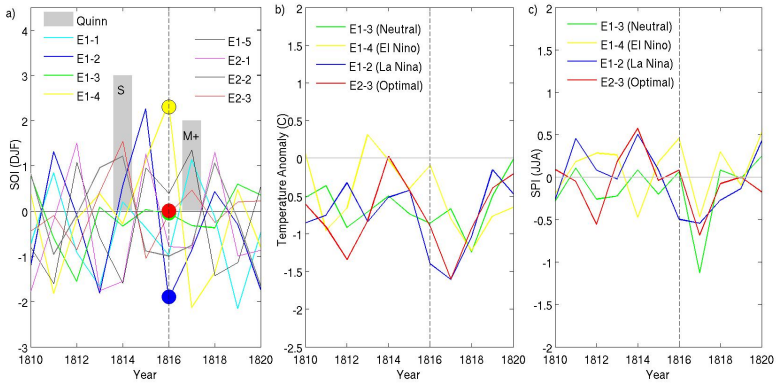

Fig. 7. ENSO (SOI) and climate in China during the cold decade of 1810 to 1820 embedding the year without summer (1816): **(a)** SOI in eight simulations of ensembles E1 and E2; grey shades indicate "strong" (S) and "moderate+" (M+) reconstructed El Niño events (see the definition by Quinn et al., 1993), these are used to define the optimal realization. Selected SOI patterns: E1-3 (neutral, green, hidden by the red symbol), E1-4 (El Niño, yellow), E1-2 (La Niña, blue), E2-3 (optimal, red); **(b)** Temperature anomalies in China for selected SOI patterns; **(c)** SPI in Southeast China, curves as in **(b)**.

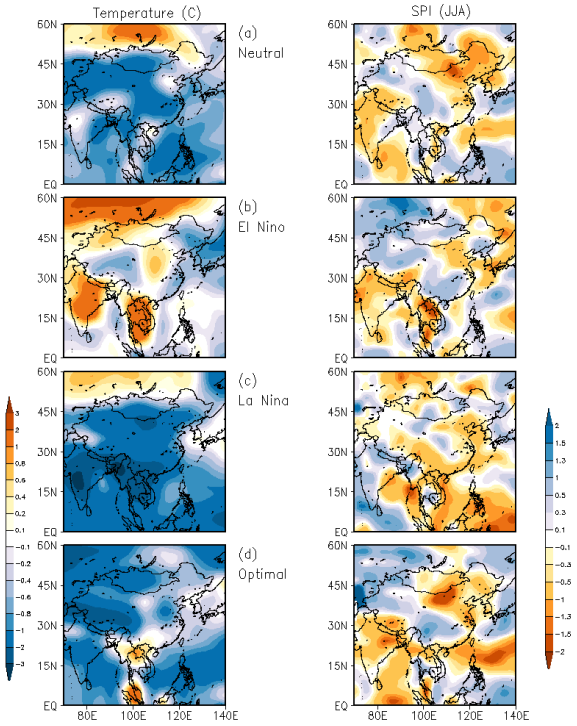

Fig. 8. Temperature anomalies in 1816 (annual mean [°C], left column) and SPI (JJA, right column) in four simulations with different SOI patterns (see also Fig. 7): **(a)** Neutral ($|\mathrm{SOI}| < 1$), **(b)** El Niño, **(c)** La Niña, and **(d)** optimal realization (compare Quinn et al., 1993).